Accepted Manuscript

3D printing of plant tissue for innovative food manufacturing: Encapsulation of alive plant cells into pectin based bio-ink

Valérie Vancauwenberghe, Victor Baiye Mfortaw Mbong, Els Vanstreels, Pieter Verboven, Jeroen Lammertyn, Bart Nicolai

PII: S0260-8774(17)30521-6

DOI: 10.1016/j.jfoodeng.2017.12.003

Reference: JFOE 9106

To appear in: *Journal of Food Engineering*

Received Date: 20 September 2017

Revised Date: 27 November 2017

Accepted Date: 6 December 2017

Please cite this article as: Vancauwenberghe, Valé., Mbong, V.B.M., Vanstreels, E., Verboven, P., Lammertyn, J., Nicolai, B., 3D printing of plant tissue for innovative food manufacturing: Encapsulation of alive plant cells into pectin based bio-ink, *Journal of Food Engineering* (2018), doi: 10.1016/j.jfoodeng.2017.12.003.

3D printing of plant tissue for innovative food manufacturing: encapsulation of alive plant cells into pectin based bio-ink

Valérie Vancauwenberghe[a], Victor Baiye Mfortaw Mbong[a], Els Vanstreels[b], Pieter Verboven[a], Jeroen Lammertyn[a], Bart Nicolai[a]

[a]*BIOSYST-MeBioS (P.V., H.K.M., B.M.N.), Biosystem department, KU Leuven, Belgium*
[b]*Rega Institute for Medical Research, KU Leuven, Leuven, Belgium*

ABSTRACT

3D food printing allows creation of foods by depositing food material according to computer aided designs. However, the number of printable materials for food is still low which limits the possibilities of creating specific structures and textures. A novel approach is tested of using food printing materials incorporating plant cells in order to print foods that resemble plant tissues in various ways. A 3D printing method was developed based on the extrusion of bio-inks composed of a low-methoxylated pectin gel and embedded lettuce leaf cells. Bovine serum albumin was added in order to increase the air fraction in the printed gel matrix. Objects containing up to 5×10^6 cells/mL were successfully 3D printed. The mechanical strength increased by the pectin concentration and decreased with the increase of air fraction and concentration of encapsulated cells. The viability of the encapsulated plant cells depended on the pectin concentration and varied from 50 to 60 %.

Keywords: additive manufacturing; encapsulation; plant cells; porosity; 3D food printing

1 INTRODUCTION

Additive manufacture (AM) constitutes an evolving group of technologies based on a digitally-controlled, robotic process and is successfully used for object manufacturing and rapid prototyping in many industrial applications [1,2]. The object is generally build up layer by layer from the bottom up from computer-assisted design (CAD) drawings by using a large variety of

materials (powder, liquid, or sheets) [1,3,4]. Recently, interest in food layer manufacturing, commonly referred to 3D food printing (3DFP), has also increased [5–7]. 3DFP fits within the concept of digital gastronomy, which combines traditional food cooking with 3D printing and aims at creating food with new structures, flavors and textures taking into account consumer organoleptic and nutritional needs [8–11]. Fused deposition, extrusion deposition and laser-sintering are the 3D printing technologies mostly used to build food structures [8]. Sugar-based objects of complex geometries were obtained through laser-sintering technology [12]. Fused deposition material and extrusion deposition technologies were used with several food products including chocolate [13,14], cookie dough [15,16], pasta dough [8] or mashed meat and vegetable with gelatin and xanthan gum as gelling agents [17,18]. Le Tohic et al. investigated how melting and extrusion during printing affected the micro-structure and textural properties of 3D printed processed cheese. They compared the properties of printed cheese products to those of untreated cheese and highlighted the impact of extrusion rates [19]. Severini et al. investigated the printability of a cereal-based dough and the mechanical and structural properties of cooked printed samples by varying the infill density and layer height [16]. Derossi et al. designed a printable fruit-based snack that was compatible with the nutritional needs of children and characterized the texture and structure properties of their food material as a function of the printing settings [20]. So far the number of food materials to be printed are still few compared to those for other food manufacturing. Moreover, the diversity of texture and structure properties of printed food remains limited as they are rarely taken into account by structure design or adjusted by using more complex printing materials. One interesting option would be the 3D printing of cells- or even artificial cells to yield foods with a cellular tissue-like structure of arbitrary design. Plant tissues are of particular interest because of their unique texture properties that are related to

both their particular porous microstructure and the turgor pressure of cells [21–24]. 3D printing of such artificial plant tissues would offer exciting possibilities to create new combinations of textures and flavours yet unseen with a large potential in personalized foods.

Here we introduce and test the idea of 3D printing of artificial plant tissues for food manufacturing using bioprinting concepts. Various bioprinting technologies have been developed to fabricate tissue constructs by means of so-called bio-inks composed of biomaterials including cells. Hydrogels are often used as biocompatible matrix material [25]. The selection and development of printing materials is based on several, sometimes conflicting criteria, including flowability (easy manipulation and extrusion), cell viability (limitation of shear stress), and final rigidity (stability of the 3D structure) [25–28]. Extrusion is appropriate for cm-scale biofabrication of cell/matrix suspensions having a high cell density and high viscosity [28,29]. However, those techniques resulted in lower cell viability in comparison to other AM method, because of shear stress occurring during the extrusion [27,28,30,31]. While great progress has been made in the development of AM technologies for biomedical applications using encapsulated human/animal mammalian cells in hydrogels, plant-derived cell types are barely described. Lode et al. [32] demonstrated that microalgae can be immobilized and cultured in a 3D alginate-based scaffolds that were constructed by extrusion deposition. In addition, scaffolds with a co-culture of human and algae cells were fabricated in which sustained delivery of oxygen or other metabolites could be provided by the micro-algae to human cells. 3D printing of land-plant cells-laden material has not received any attention yet.

In a previous study, we reported that low methoxylated (LM) pectin gel can be a promising food-ink for the 3D printing of customizable water-based porous food. The formulation of pectin food-inks was adjusted by changing the pectin, sugar syrup or bovine serum albumin (BSA)

concentration in order to obtain edible printed constructs having variable microstructure and texture properties. [33]. The gelation of the LM pectin food-ink is generated through the formation of calcium crosslinks between free carboxyl groups [34,35]. The addition of Ca^{2+} was required and adjusted according to the stoichiometric ratio ($R = 2[Ca^{2+}]/[COO^{-}]$) in order to obtain suitable flowability of the gel [33]. Owing to its cytocompatibility and the possibility to tune its properties, pectin makes it a suitable candidate for delivery systems and scaffold materials in food and biomedical applications [36–38]. Further, pectin is the obvious choice of matrix material as it is the main constituent of the middle lamella in plant tissues that glues cells together [39,40].

The objective of this work was to proof that a high amount of plant cells and air bubbles can be successfully encapsulated into pectin-based bio-inks and then 3D printed at room temperature by an extrusion based method. We also wanted to show that it is possible to 3D print objects with variable texture and porosity. We focused on the use of cells isolated from plant tissue (leafs) as an ingredient in 3D printed foods. The culture of such cells was beyond the scope of this article.

2 MATERIALS & METHODS

Table 1 presents a timeline overview of the multiple steps necessary to print objects having encapsulated plant cells. Those steps include the production of the cell suspension, the preparation of the bio-ink, the 3D printing process, and, finally, the methods used to characterize the printed objects. All production steps are detailed in the following sections.

2.1 Gel ingredients and reagents

The following ingredients were used for the pectin solution: high methoxylated pectin from citrus peel (≥ 74% Galacturonic acid, Sigma-Aldrich P9135), calcium chloride dihydrate (Chem-

Lab, cat. no. CL00.0317.1000). The following reagents were used for the maceration and buffer solutions: D-glucose anhydrous (VWR, cat. no. 0188), 4-morpholineethanesulfonic acid hydrate (MES, pH 5.8; Sigma Aldrich, cat. no. M2933), magnesium sulphate heptahydrate (Sigma Aldrich, cat. no. M5921), bovine serum albumin (BSA, Sigma Aldrich, cat. no. A7906), pectinase from Aspergillus niger (Sigma Aldrich, cat. no. 17389). For viability characterization we used: Evans blue (Fluka, cat. no.46160), fluorescein diacetate (Sigma Aldrich, cat. no. F1397), and Hoechst 33258, pentahydrate (bis-benzimide) (Life Technologies, cat. no. H1398).

2.2 Solution preparation

Low methoxylated pectin having a degree of methoxylation of 12 ± 0.5 % was produced from high methoxylated (HM) pectin by the saponification method described by Vancauwenberghe et al [33]. HM pectin solution was set at pH of 11 and titrated with 2M NaOH for 1 h at 17 °C. The degree of methoxylation was determined by infrared spectrometry following the protocol of Kyomugasho et al. [43]. For the Lamb's lettuce cell isolation, a maceration solution of 240 mM glucose, 15 mM MES buffer pH 5.8, 2 mM $MgSO_4$ and 1% (w/v) pectinase was prepared. The solution was incubated at 55 °C for 10 min to activate the pectinase and put on ice for 10 min to cool to room temperature. Then, 3 mM $CaCl_2$ and 0.2% (w/v) BSA were added to the maceration solution.

An isotonic glucose buffer (240 mM glucose, 15 mM MES buffer pH 5.8, 2 mM $MgSO_4$, 3 mM $CaCl_2$) containing 0 or 2 % (w/v) BSA was used as solvent to prepare the solutions necessary for the bio-ink preparation, 3D printing and viability test:

- The pectin solutions: 30 or 70 g/L LM-pectin with and without 0.2% (w/v) BSA

- The $CaCl_2$ solutions: 26 or 40 mM $CaCl_2$ with and without 0.2% (w/v) BSA
- The post-treatment solutions: 50 mM $CaCl_2$ with and without 0.2% (w/v) BSA
- The Evans blue solution: 0.5 % (w/v) Evans blue and 0.2% (w/v) BSA

Stock solutions of 1% (w/v) fluorescein and 1% (w/v) Hoechst were prepared in acetone and distilled water, respectively.

All the solutions were prepared the day before the lettuce cell isolation and were kept at 4°C.

2.3 Lamb's lettuce cells isolation and viability test prior printing

According to the protocol developed by Baiye Mfortaw Mbong et al. [44], Lamb's lettuces cells (*Valerianella locusta*, L. var. 'Gala') were isolated from commercially mature plants with fully-developed leaves provided by a commercial grower (Duffel, Belgium). To prepare about 20 mL of bio-ink, 8 flasks of 30 mL maceration solution containing 15 striped leaves each were prepared and then, vacuum infiltrated for 15 min. Finally, the leaves were incubated in the maceration solution in the dark for 1.5 h at 20 °C while flushed with air (21 kPa O_2, 0 kPa CO_2, at 15 L/h). The isolation was performed in two batches of 16 flasks: one batch was used to prepare the bio-inks made of 15 g/L pectin, the other one for the bio-inks made of 35 g/L pectin.

After the isolation process, the suspension was filtered through a nylon mesh (pore size 35–75 mm) in 2 beakers of 250 mL. The filtrate was washed with equal amount of isotonic glucose buffer and decanted after a few minutes. The process of decanting was repeated three times. The suspension was finally poured in equal volume in four falcon tubes (50 mL) and was decanted overnight at 1 °C.

Live and dead cells were evaluated by the Evans Blue Exclusion staining technique [45,46]. The cell suspension (50 µL) was stained with few drops of Evans blue solution for 30 seconds at

room temperature (20 °C) which stains the dead cells. The percentages of dead and live cells were determined by counting on a haemocytometer under a light microscope (BX40-Olympus, Japan).

2.4 Bio-ink preparation

The bio-ink consisted of the mixing of a pectin solution with a cell/$CaCl_2$ suspension (1:1). Eight different bio-inks with and without embedded lettuce cells were prepared varying the pectin and BSA concentrations in order to change the viscosity and the porosity of the food-ink respectively. Their composition is given in Table 2.

Before the preparation of 20 mL bio-ink, 10 mL pectin solution was mixed for 10 min under 10000 rpm stirring (IKA® T25 Digital Ultra-Turrax, head size 18 mm) resulting in the incorporation of air bubbles which were stabilized if BSA was in solution [33]. After the high speed stirring, the pectin solution was stirred under magnetic stirring. 2x 10 mL of lettuce cell suspension were collected from 2 falcon tubes of raw suspension decanted overnight, and washed with the same volume of 26 mM or 40 mM $CaCl_2$ solution. The resulting cell/$CaCl_2$ suspensions containing 13 mM or 20 mM $CaCl_2$, were decanted for 20 min and the viability was estimated by the Evans Blue Exclusion staining technique. Then, 5 mL of each falcon tube of cell/$CaCl_2$ suspension was added into the pectin solution drop by drop. The mixing of the pectin solution with cell/$CaCl_2$ suspension resulted immediately in the formation of a gel having the composition listed in Table 2. The bio-ink was gently stirred with a spatula for 5 min before being transferred to the syringe. The bio-inks containing 0 % (v/v) cell suspension were prepared in a similar manner.

Some chemicals used in this step were not edible-grade. For this reason, we preferred using the term “bio-ink” instead of “food-ink”. More focus on the food-grade material selection will be addressed in future research.

2.5 3D printing and post-treatments

The 3D printing process based on extrusion deposition at room temperature (23 °C) has been described previously [33]. The 3D printer prototype consisted of a 3D robotic system (CNC Bench 3D 4046, GoCNC.de, Germany), control software (WinPN-CN USB, Lewetz, Germany), a pressure system and an injection device. A syringe pump (Harvard Apparatus, Holliston, MA, USA) was used as a pressure system to provide a precise continuous extrusion flow rate. The STL files were designed and exported using AutoCAD (AutoCAD; Autodesk, Cupertino, CA, USA). The open-source CAM software Slic3r (slic3r.org, consulted on February 2015) was used to generate the G-code files, providing the XYZ pathway instructions of the printer, from the STL file. The following printing setting were used: extrusion nozzle diameter of 0.838 mm, layer height of 0.838 mm, extrusion flow rate of 0.34 mL/min and infill velocity of 10 mm/s. The shear rate ($\dot{\gamma}$) during the extrusion printing was calculated according to Eq. 1 [47]:

$$\dot{\gamma} = \frac{8\bar{v}}{d} = \frac{8Q}{d \cdot A} \qquad \text{Eq. 1}$$

where $\bar{v}$ is the average velocity (mm/s), d is the nozzle diameter (mm), Q is the extrusion flow rate (mm^3/s) and A (mm^2) is the cross-sectional area of the nozzle, It was found to be equal to 21.8 s^{-1}.

Cubes of 1.5 cm edge were printed for visual comparison and mechanical characterization. The cubical geometry allowed an easy qualification of the printability and build quality features

(shape reliability, edge aspect, material layering) and simplified the mechanical characterization. Then, thin square layers of 1.5 x 1.5 x 0.25 cm^3 were printed for the cell density and viability estimation by confocal microscopy. Finally, cubes of 0.7 cm edge were printed for the structural characterization by micro computed tomography (CT).

After the printing, the cubes of 1.5 cm and 0.7 cm edge were incubated into the post-treatment solution for 60 and 30 min, respectively. This post treatment was required to solidify the pectin gel and let the Ca^{2+} ions diffuse through the gel. The square layers were incubated into the post-treatment solution composed of 50 mM $CaCl_2$, 10 µg/mL Hoechst stock solution and 1.5 µg/mL fluorescein diacetate stock solution for 30 min in the dark. Hoechst 33258 stained cell nuclei and protoplasts of dead and damaged cells because of their low permeability [48,49]. Fluorescein diacetate stained alive cells [50].

2.6 Confocal microscopy and image analysis

The same day of 3D printing, the square layer objects were analyzed using a Leica TCS SP5 confocal microcope (Leica Microsystems, Germany). Fluorescence pictures (512 x512 pixels) were recorded using a HCX PL APO CS 20x (NA: 0.70) objective. Hoechst 33258 was detected using 405 nm excitation and emission wavelengths between 410 and 460 nm, fluorescein diacetate and chloroplasts were imaged after 488 nm excitation and emission detection between 493 and 550 nm, and 584 and 666 nm, respectively. Z-stacks of 90 cross-sections with a 1 µm step-size and an area of 775 µm × 775 µm were obtained. The brightness and contrast of the recorded images were improved using ImageJ software (U.S. NIH, Bethesda, MD).

The cell viability and distribution in the confocal image stacks with a prismatic volume of 90 µm × 775 µm × 775 µm were visualized and characterized using the Avizo image processing

205 software (version 9.0.1, VSG, France). The workflow of the image processing (Figure 1)
206 included color deconvolution followed by median filtering. Then, the color channels were
207 binarized and separated by interactive thresholding. The red, green and blue (RGB) channels
208 corresponded, respectively, to chloroplasts, fluorescein diacetate and Hoechst 33258 stains. RGB
209 channels were superposed by using "OR" operation to visualize the complete cell distribution
210 while avoiding the counting of overlapping objects. The resulting stack was despeckled by
211 morphological closing and opening operations. Finally, the aggregated cells were separated with
212 a watershed algorithm and the cell count was obtained by 3D analysis. The G channel was used
213 separately to count the viable cells by using the same processing workflow (see Figure 1). The
214 density of cells d (cells/mL) was calculated as the total number of object obtained by the image
215 processing of RGB channels, divided by the image stack volume. The cell viability v (%) was
216 obtained from the division of the amount of viable cells obtained by the image processing of the
217 G channel by the total amount of cells calculated by the image processing of RGB channels.

218 2.7 X-ray micro-CT and image analysis

219 The day after 3D printing, X-ray CT was performed to visualize the porous microstructure of the
220 printed cubes of 0.7 cm edge using a Skyscan 1172 (Bruker microCT, Belgium). Micro-CT
221 settings were set at a source voltage of 60 kV, a source current of 167 µA with pixel image
222 resolution of 4.87 µm. A radiographic image of 1048 by 2000 pixels was acquired with an
223 averaging of 3 frames for each rotation step of 0.3° over 180°. The projection images were
224 reconstructed using NRecon software (version 1.6.10.2, Bruker microCT, Belgium).

225 The reconstructed images were analyzed using the CTAn software (Bruker microCT, Belgium)
226 to determine the porosity (ϕ). All image datasets were trimmed to a circular region of 1150 pixel
227 diameter in order to perform the analysis on a cylindrical volume of 2.80 mm of radius and 4.56

mm of height. The sliced images were treated with a median filtering, an automatic thresholding by the Otsu method and, finally, closing and opening morphological operations with a radius of two pixels. The workflow of the image processing is summarized in Figure 2.

2.8 Mechanical characterization

The day after 3D printing, the printed cubes of 1.5 cm edge were physically characterized by force-deformation measurements using a TA.XTPlus texture analyzer device with a cylindrical metal compression plate of 75 mm diameter (Stable Microsystems, Godalming, UK). The compression test was performed with a load force of 0.5 N and maximal strain of 80 % at a speed of 1 mm/s. The engineering Young's modulus E was determined by the slope of the linear part of the stress-strain curves [51]. The linear part was estimated by the line of best fit obtained from the stress-strain curve having a constant coefficient of regression of more than 0.98. This corresponded to a strain (ε) interval of [0.02, 0.12] for samples composed of 15 g/L pectin and [0.05, 0.15] for samples composed of 35 g/L pectin.

The maximum compressive stress or yield stress (Y) was also estimated as an indicator of the gel strength [52,53]. It was defined as the point at the stress/strain curve where a drop or no increase in stress occurred with an increase in strain [54]. In the case of large deformations such as during yielding, true strains and stresses should be considered. However, common expressions for true stresses and strains are based on conservation of volume which is not assured here because of the high air fraction of some samples [55]. We, therefore, used the engineering stress and strain to estimate the yield stress.

2.9 Statistics

The bio-inks were prepared in one batch and the confocal microscopy, micro-CT and compression test were performed in triplicate. For all measurements and bio-ink compositions, the mean value ± standard error was calculated. The mean values were analyzed through t-test at confidence level of 95 % in order to highlight the significance and independence of the investigated parameters on measured properties.

3 RESULTS AND DISCUSSION

3.1 3D printing

The bio-inks were successfully 3D printed using the printing parameters established by Vancauwenberghe et al. [33]. The bio-ink deposition and the 3D structure stability during and after printing were carefully observed in order to estimate the build quality. This observation is shown in Figure 3 which compares the printed cubes of 1.5 cm edge. For all the bio-ink compositions, the deposition occurred regularly according to visual observation. The edges of printed objects were manually measured and compared to the design. The manufactured objects kept their 3D shape without spreading, leading to a good printing accuracy. However, the edges measuring 1.3 cm in average were slightly smaller than expected. This difference could be due to the syneresis of the pectin gel which was caused by slow shrinking of pectin chains upon increasing of the Ca^{2+} ion concentration after the post-treatment. This resulted in a release of water from the gel involving a decrease in its volume dimensions [56,57]. This effect was probably independent of bio-ink composition as the dimensions of all printed samples with and without embedded cells were in average the same. We can also established based on the independence of bio-ink composition on shape dimensions that the encapsulated lettuce cells did not affect significantly the bio-ink flowability adjusted by the stoichiometric ratio of pectin/Ca^{2+}

gel ($R = 2[Ca^{2+}]/[COO^-]$) [33]. The R-value corresponded respectively to 0.38 and 0.22 for the bio-inks made of 15 g/L and 35 g/L pectin. After the post-treatment, the printed objects were solid enough to be easily manually handled for the characterization tests as they kept their structural integrity through these manipulations.

We could examine the build quality from the layering ripples of the printed objects (Figure 3). They appeared uniformly straight for all printed objects with the exception of samples made of 35g/L pectin with encapsulated cells which got ripples with a very slight curvature. This was probably due to swelling effect during the post treatment [33]. The colour of the printed cubes varied with the composition of the bio-ink: the pectin gel gave a yellowish colour to the samples while the green colour was provided by the chloroplasts of the lettuce cells. The printed cubes composed of BSA had a lighter colour indicating the presence of air bubbles that caused light scattering [58].

3.2 Characterization of the porosity

The porosity or air fraction of the 3D printed cubes of 0.7 cm edge was obtained from the structural analysis of the X-ray CT scans. The acquired 2D slices are compared in Figure 4. The black spots on the CT cross-sections represent air bubbles which are surrounded by the pectin gel with or without embedded cells in grey scale. Lettuce cells and the pectin medium cannot be distinguished on the CT slices as both materials have a mass density close to water and, thus, a similar x-ray attenuation coefficient [59,60].

An increase of the porosity is clearly noticed for the printed samples containing BSA as reported in Table 3. Particularly, the porosity of samples made of 15 g/L pectin and 2 g/L BSA with and without 50 % (v/v) embedded plant cells increased to 20 % while it only slightly increased for

293 samples the samples made of 35 g/L pectin and 2 g/L BSA with and without embedded plant
294 cells. As already discussed previously [33], the incorporation of air bubbles is promoted by high
295 stirring of the bio-ink before printing. In addition, the foam is stabilized by the adsorption of
296 BSA proteins at the air-liquid interface [61,62]. The gel state of the bio-inks reduced the air
297 bubbles motion and coalescence [63–65]. For this study, the high stirring was performed on the
298 30 g/L or 70 g/L pectin solutions before mixing with the lettuce cell/$CaCl_2$ suspension in order to
299 prevent cell damage. Those solutions were prepared using isotonic glucose buffer as solvent
300 which contained only 3mM $CaCl_2$. This low Ca^{2+} concentration resulted in stoichiometric R-
301 values of 0.1 and 0.05 for 30 g/L and 70 g/L pectin solutions, respectively, and was probably not
302 sufficient to significantly increase the viscosity of the solution [66]. This made the solution more
303 susceptible to foam collapse especially in the case of the 70 g/L pectin solution. The
304 encapsulated cells in bio-ink led to a slight decrease in the porosity of the printed object. Due to
305 the complex formulation of the bio-inks comprising three distinct phases (air, gel and plant
306 cells), the variation of the porosity was difficult to interpret. The embedded cells may affect the
307 adsorption rate of the protein at the air-liquid interface. Several factors may be responsible of this
308 change including change of the visco-elastic properties [67,68] or additional interactions between
309 BSA and cell wall [62,69,70].

310 3.3 Mechanical properties obtained by compression tests

311 The mechanical properties were estimated from the stress-strain curve obtained by performing
312 compression test on the printed cubes of 1.5 cm edge. Examples of the stress-strain response for
313 each sample and the estimation of the Young's modulus and yield stress are given in Figure 5.
314 For the printed samples made of 15 g/L pectin, the Young's modulus varied between 30 and 65
315 kPa and the yield stress varied from 5 to 10 kPa. Samples made of 15 g/L pectin with

316 encapsulated cells had lower values of the mechanical properties in comparison to the reference
317 samples made of 15 g/L pectin suggesting that the encapsulated cells affected those properties
318 negatively. However, similar stress-strain responses were found for the samples made of 15 g/L
319 pectin and 2 g/L BSA with and without 50 % (v/v) embedded plant cells with values of the
320 Young's modulus and yield stress that were statistically equivalent. Those samples had lower
321 values of mechanical properties in comparison to the sample composed of 15 g/L pectin with and
322 without encapsulated cells due to their high porosity which tended to disrupt the continuity of the
323 cell/gel mixture [71]. The presence of cells did not impact significantly the mechanical properties
324 for such high porosity. The printed samples made of 35 g/L pectin resulted in higher values of
325 mechanical properties with Young's moduli varying from 140 to 200 kPa and yield stresses
326 varying from 30 to 90 kPa. The increase of pectin concentration in the bio-ink involved higher
327 mechanical strength because of a denser cross-linked network as discussed in Vancauwenberghe
328 et al. [33]. For those samples, the reference printed cubes made of 35 g/L pectin with and without
329 2g/L BSA, gave similar mechanical behavior under compression in comparison to the printed
330 cubes composed of 35 g/L pectin having embedded cells with and without 2g/L BSA. The
331 encapsulated cells clearly influenced the mechanical properties of printed object more than the
332 trapped air bubbles because the air fraction was not sufficient enough to affect the continuity of
333 the gel matrix [71,72]. The printed samples containing embedded cells can be considered as
334 composite material in which the LM-pectin/Ca^{2+} gel was the matrix and the lettuce cells were
335 particulate filler. A simple description of the mechanical properties of composite material is the
336 rule of mixtures in which the properties of composite material are computed as the weighted
337 mean of the properties of matrix and filler material [73–75]. According to this general rule, the
338 embedded cells would have lower mechanical properties than the pectin matrix. This would lead

to a decrease of Young's modulus for the printed objects having encapsulated cells. In addition, the decrease of the bio-yield stress would suggest that the lettuce cell were unbound to the pectin matrix according to the Nielsen theory (1966) [76]. However, BSA may affect positively the adhesion of the lettuce cells into the pectin matrix because samples made of 15 g/L and 35 g/L pectin with 2 g/L BSA and 50% (v/v) embedded cells had mechanical properties closer to their respective reference. However, the actual results are not sufficient to confirm this observation. More investigations would be necessary to specify the impact on the mechanical properties induced by the encapsulated plant cells into pectin matrix with and without BSA.

3.4 Cell density and viability

After each isolation of Lamb's lettuce cells, the cell viability was determined by counting dead and alive cells by the Evans blue exclusion staining technique. Two batches of cell suspension were produced: one for the bio-inks made of 15 g/L pectin and the other one for bio-inks made of 35 g/L pectin. The viability, given by Table 4, was around 85 % for each suspension after the isolation process which was an acceptable efficiency for further manipulation. The day after, the cell suspensions were decanted into $CaCl_2$ solutions of 13 mM or 20 mM in order to produce bio-inks made of 15 g/L or 35 g/L pectin, respectively. Note that the $CaCl_2$ solutions were prepared using a glucose osmotic buffer as solvent in order to maintain the osmotic equilibrium of the cells (see §2.2). After the decantation of 20 min, the viability was evaluated again in order to qualify the effect of $CaCl_2$. From the results presented in Table 4, we observed a decrease of a few percent in the cell viability after the 20 min of decantation which was independent of the $CaCl_2$ concentration. The viability of the cell suspensions remained relatively high before being mixed to the pectin solutions.

Figure 6 reports the cell viability and density after 3D printing obtained from the image analysis of confocal microscope scans. In general, the viability of the printed objects varied from 50 to 60 %. This is a promising results as the 3D printing of encapsulated land-plant cells has never been tried so far. Moreover, for the first time, cells of large size (± 40 µm diameter) were used for 3D printing application. Samples composed of 15 g/L pectin and encapsulated cells with and without BSA had the highest viability which was independent of the addition of BSA. The increase of pectin concentration seemed to affect the viability as shown in Figure 6. Bio-inks made of 35 g/L pectin resulted in gels of higher visco-elastic properties which probably impacted the shear stress during extrusion, and, thus, increased cell damage [25,77–79]. The density remained the same for all samples (5×10^6 cells/mL) with the exception of samples composed of 15 g/L pectin, 2 g/l BSA and 50 % (v/v) lettuce cells, having a density of 4×10^6 cells/mL. This difference was obviously because of the higher air fraction of those samples. Finally, the distribution of cells appeared homogeneous for alive and dead cells which did not form clusters as shown in Figure 7. The method developed to encapsulate plant cell into pectin was successful and reproducible for variable gel composition. However, at this stage of the research, the printed object did not have cell density comparable to those of plant tissues which may be up to $10^7 – 10^8$ cells/mL [80–82].

4 CONCLUSION AND PERSPECTIVES

This research successfully tested the concept of 3D printing of alive plant cells. For the first time, we showed that land-plant cells can be encapsulated in pectin gels at high density and can be 3D printed with good accuracy and reproducibility. The formulation of bio-ink at different pectin concentration and the 3D printing process did not dramatically alter the cell viability. However, the increase of the pectin concentration resulted in lower viability due to the higher viscosity of

384 such bio-ink. The encapsulation of cells in bio-ink tended to decrease the mechanical and
385 structural properties of the printed object in comparison to their reference results. More
386 investigations would be necessary to understand the effect of encapsulated plant cells on these
387 properties.

388 The methodology presented in this study may be considered as a first step to produce 3D printed
389 cellular or particulate foods. Nevertheless, further research would be necessary before being able
390 to manufacture cellular edible material having similar properties than real plant tissue. Future
391 research should address exploring the formulation by encapsulating different kind of filler which
392 can be plant cells, pulps or artificial micro-particles. Notably, methods to increase the cell
393 density would be required to get microstructure closer to those of plant tissue. Several ways can
394 be tried to reach that objective including the improvement of printing method or the culture of
395 cells. More attention on the edibility of the products and consumer acceptance should also be
396 addressed as a final step to validate the method and to develop more variety of products.

397 **REFERENCES**

398 [1] Getschmann C. Research Trends in Media Informatics. In: Villa Eberhardt U, editor. 3D
399 Print. Technol. Appl., 2013, p. 91–8.
400 [2] Berman B. 3-D printing: The new industrial revolution. Bus Horiz 2012;55:155–62.
401 doi:10.1016/j.bushor.2011.11.003.
402 [3] Gibson I, Rosen DW, Stucker B. Additive Manufacturing Technologies. vol. 76. Boston,
403 MA: Springer US; 2010. doi:10.1007/978-1-4419-1120-9.
404 [4] Rengier F, Mehndiratta A, Von Tengg-Kobligk H, Zechmann CM, Unterhinninghofen R,
405 Kauczor HU, et al. 3D printing based on imaging data: Review of medical applications.
406 Int J Comput Assist Radiol Surg 2010;5:335–41. doi:10.1007/s11548-010-0476-x.
407 [5] Lipton JI, Cutler M, Nigl F, Cohen D, Lipson H. Additive Manufacturing for the Food
408 Industry - A review. Trends Food Sci Technol 2015;43:114–23.
409 doi:10.1016/j.tifs.2015.02.004.
410 [6] Godoi FC, Prakash S, Bhandari BR. 3d printing technologies applied for food design:
411 Status and prospects. J Food Eng 2016;179:44–54. doi:10.1016/j.jfoodeng.2016.01.025.
412 [7] Wegrzyn TF, Golding M, Archer RH. Food Layered Manufacture: A new process for
413 constructing solid foods. Trends Food Sci Technol 2012;27:66–72.
414 doi:10.1016/j.tifs.2012.04.006.
415 [8] TNO. 3D Printing: now printing food too 2012.

https://www.youtube.com/watch?v=x6WzyUgbT5A (accessed October 1, 2017).
[9] Food Factory of the Future. Digital Factory. Belgium 2013.
[10] Sun J, Peng Z, Zhou W, Fuh JYH, Hong GS, Chiu A. A Review on 3D Printing for Customized Food Fabrication. Procedia Manuf 2015;1:308–19. doi:10.1016/j.promfg.2015.09.057.
[11] Zoran A, Coelho M. Cornucopia : The Concept of Digital Gastronomy. Leonardo 2011;44:425–31. doi:10.1162/LEON_a_00243.
[12] CandyFab. The CandyFab project 2009. http://candyfab.org/ (accessed June 29, 2017).
[13] Causer C, Butcher S, Henderson J, Iggulden G. They've got a golden ticket. IEEE Potentials 2009;28:42–4. doi:10.1109/MPOT.2009.933608.
[14] Hao L, Mellor S, Seaman O, Henderson J, Sewell N, Sloan M. Material characterisation and process development for chocolate additive layer manufacturing. Virtual Phys Prototyp 2010;5:57–64. doi:10.1080/17452751003753212.
[15] Valérie Vancauwenberghe, Delele MA, Aregawi W, Verboven P, Bongaers E, Noort M, et al. Characterization and model-based design validation of 3D printed cookies. 7th Conf. Ind. Comput. Tomogr., Leuven, Belgium: 2017.
[16] Severini C, Derossi A, Azzollini D. Variables affecting the printability of foods: Preliminary tests on cereal-based products. Innov Food Sci Emerg Technol 2016;38:281–91. doi:10.1016/j.ifset.2016.10.001.
[17] Cohen DL, Malone E, Lipson H, Bonassar LJ. Direct freeform fabrication of seeded hydrogels in arbitrary geometries. Tissue Eng 2006;12:1325–35. doi:10.1089/ten.2006.12.1325.
[18] Lipton J, Arnold D, Nigl F, Lopez N, Cohen D, Noren N, et al. Multi-Material Food Printing with Complex Internal Structure Suitable for Conventional Post-Processing. SOLID Free. Fabr. PROCEEDINGS; Int. Solid Free. Fabr. Symp. 21st, Int. Solid Free. Fabr. Symp., Austin: 2010, p. 809–15.
[19] Le Tohic C, O'Sullivan JJ, Drapala KP, Chartrin V, Chan T, Morrison AP, et al. Effect of 3D printing on the structure and textural properties of processed cheese. J Food Eng 2016. doi:10.1016/j.jfoodeng.2017.02.003.
[20] Derossi A, Caporizzi R, Azzollini D, Severini C. Application of 3D printing for customized food. A case on the development of a fruit-based snack for children. J Food Eng 2016:1–11. doi:10.1016/j.jfoodeng.2017.05.015.
[21] Tyree MT, Jarvis PG. Water in Tissues and Cells. Physiol. Plant Ecol. II, Berlin, Heidelberg: Springer Berlin Heidelberg; 1982, p. 35–77. doi:10.1007/978-3-642-68150-9_3.
[22] Falk S, Hertz CH, Virgin HI. On the Relation between Turgor Pressure and Tissue Rigidity. I. Experiments on Resonance Frequency and Tissue Rigidity. Physiol. Plant., vol. 11, 1958, p. 802–17. doi:10.1111/j.1399-3054.1958.tb08274.x.
[23] Oey ML, Vanstreels E, De Baerdemaeker J, Tijskens E, Ramon H, Hertog MLATM, et al. Effect of turgor on micromechanical and structural properties of apple tissue: A quantitative analysis. Postharvest Biol Technol 2007;44:240–7. doi:10.1016/j.postharvbio.2006.12.015.
[24] Alamar MC, Vanstreels E, Oey ML, Moltó E, Nicolaï BM. Micromechanical behaviour of apple tissue in tensile and compression tests: Storage conditions and cultivar effect. J Food Eng 2008;86:324–33. doi:10.1016/j.jfoodeng.2007.10.012.
[25] Malda J, Visser J, Melchels FP, Jüngst T, Hennink WE, Dhert WJA, et al. 25th

anniversary article: Engineering hydrogels for biofabrication. Adv Mater 2013;25:5011–28. doi:10.1002/adma.201302042.

[26] Mironov V, Reis N, Derby B. Review: Bioprinting: A Beginning. Tissue Eng 2006;12:631–4. doi:10.1089/ten.2006.12.631.

[27] Li J, Chen M, Fan X, Zhou H. Recent advances in bioprinting techniques : approaches , applications and future prospects. J Transl Med 2016:1–15. doi:10.1186/s12967-016-1028-0.

[28] Hong N, Yang G, Lee J, Kim G. Review Article 3D bioprinting and its in vivo applications 2017:1–16. doi:10.1002/jbm.b.33826.

[29] Wüst S, Müller R, Hofmann S. Controlled Positioning of Cells in Biomaterials—Approaches Towards 3D Tissue Printing. vol. 2. 2011. doi:10.3390/jfb2030119.

[30] Derby B. Printing and prototyping of tissues and scaffolds. Science 2012;338:921–6. doi:10.1126/science.1226340.

[31] Ferris CJ, Gilmore KJ, Wallace GG, Panhuis M in het. Modified gellan gum hydrogels for tissue engineering applications. Soft Matter 2013;9:3705–11. doi:10.1039/C3SM27389J.

[32] Lode A, Krujatz F, Brüggemeier S, Quade M, Schütz K, Knaack S, et al. Green bioprinting: Fabrication of photosynthetic algae-laden hydrogel scaffolds for biotechnological and medical applications. Eng Life Sci 2015;15:177–83. doi:10.1002/elsc.201400205.

[33] Vancauwenberghe V, Katalagarianakis L, Wang Z, Meerts M, Hertog M, Verboven P, et al. Pectin based food-ink formulations for 3-D printing of customizable porous food simulants. Innov Food Sci Emerg Technol 2017;42:138–50. doi:10.1016/j.ifset.2017.06.011.

[34] Fraeye I, Colle I, Vandevenne E, Duvetter T, Van Buggenhout S, Moldenaers P, et al. Influence of pectin structure on texture of pectin–calcium gels. Innov Food Sci Emerg Technol 2010;11:401–9. doi:10.1016/j.ifset.2009.08.015.

[35] Willats WG., Knox JP, Mikkelsen JD. Pectin: new insights into an old polymer are starting to gel. Trends Food Sci Technol 2006;17:97–104. doi:10.1016/j.tifs.2005.10.008.

[36] Munarin F, Tanzi MC, Petrini P. Advances in biomedical applications of pectin gels. Int J Biol Macromol 2012;51:681–9. doi:10.1016/j.ijbiomac.2012.07.002.

[37] Matalanis A, Jones OG, McClements DJ. Structured biopolymer-based delivery systems for encapsulation, protection, and release of lipophilic compounds. Food Hydrocoll 2011;25:1865–80. doi:10.1016/j.foodhyd.2011.04.014.

[38] Moreira HR, Munarin F, Gentilini R, Visai L, Granja PL, Tanzi MC, et al. Injectable pectin hydrogels produced by internal gelation: PH dependence of gelling and rheological properties. Carbohydr Polym 2014;103:339–47. doi:10.1016/j.carbpol.2013.12.057.

[39] Van Buren JP. Function of Pectin in Plant Tissue Structure and Firmness. Chem. Technol. Pectin, Elsevier; 1991, p. 1–22. doi:10.1016/B978-0-08-092644-5.50006-6.

[40] Sila DN, Van Buggenhout S, Duvetter T, Fraeye I, De Roeck A, Van Loey A, et al. Pectins in Processed Fruits and Vegetables: Part II-Structure-Function Relationships. Compr Rev Food Sci Food Saf 2009;8:86–104. doi:10.1111/j.1541-4337.2009.00071.x.

[41] Luckwill LC. Studies of Fruit Development in Relation to Plant Hormones: IV. Acidic Auxins and Growth Inhibitors in Leaves and Fruits of the Apple. J Hortic Sci 1957;32:18–33. doi:10.1080/00221589.1957.11513885.

[42] Davies PJ. The Plant Hormones: Their Nature, Occurrence, and Functions. Plant Horm., Dordrecht: Springer Netherlands; 2010, p. 1–15. doi:10.1007/978-1-4020-2686-7_1.

[43] Kyomugasho C, Christiaens S, Shpigelman A, Van Loey AM, Hendrickx ME. FT-IR spectroscopy, a reliable method for routine analysis of the degree of methylesterification of pectin in different fruit- and vegetable-based matrices. Food Chem 2015;176:82–90. doi:10.1016/j.foodchem.2014.12.033.

[44] Mbong VBM, Ampofo-Asiama J, Hertog MLATM, Geeraerd AH, Nicolai BM. The effect of temperature on the metabolic response of lamb's lettuce (Valerianella locusta, (L), Laterr.) cells to sugar starvation. Postharvest Biol Technol 2017;125:1–12. doi:10.1016/j.postharvbio.2016.10.013.

[45] Shipway MR, Bramlage WJ. Effects of carbon dioxide on activity of apple mitochondria. Plant Physiol 1973;51:1095–8. doi:10.1104/pp.51.6.1095.

[46] Puschmanni R, Romani R. Ethylene Production by Auxin-Deprived, Suspension-Cultured Pear Fruit Cells in Response to Auxins, Stress, or Precursor. Plant Physiol 1983;70:1013–9. doi:http://dx.doi.org/10.1104/pp.73.4.1013.

[47] Darby R. Chemical Engineering Fluid Mechanics, Revised and Expanded. 2001.

[48] Meadows MG, Potrykus I. Hoechst 33258 as a vital stain for plant cell protoplasts. Plant Cell Rep 1981;1:77–9. doi:10.1007/BF00269279.

[49] Laloue M, Courtois D, Manigault P. Convenient and rapid fluorescent staining of plant cell nuclei with 33258 Hoechst. Plant Sci Lett 1980;17:175–9. doi:10.1016/0304-4211(80)90145-5.

[50] Widholm JM. The use of Fluorescein Diacetate and Phenosafranine for determining viability of cultured plant cells. Stain Technol 1972;47:189–94. doi:10.3109/10520297209116483.

[51] Willats WGT, Orfila C, Limberg G, Christian H, Alebeek GWM Van, Voragen AGJ, et al. Modulation of the Degree and Pattern of Methyl-esterification of Pectic Homogalacturonan in Plant Cell Walls 2001;276:19404–13. doi:10.1074/jbc.M011242200.

[52] Endress H-U, Mattes F. Rheological Characterization of Gum and Jelly Products. Adv. Pectin Pectinase Res., Dordrecht: Springer Netherlands; 2003, p. 449–65. doi:10.1007/978-94-017-0331-4_33.

[53] Sahin S, Sumnu SG. Rheological Properties of Foods. Phys. Prop. Foods, New York, NY: Springer New York; 2006, p. 39–105. doi:10.1007/0-387-30808-3_2.

[54] Lu R, Abbott JA. Force/deformation techniques for measuring texture. Texture Food, Elsevier; 2004, p. 109–45. doi:10.1533/978185538362.2.109.

[55] Roeder RK. Mechanical Characterization of Biomaterials. Elsevier; 2013. doi:10.1016/B978-0-12-415800-9.00003-6.

[56] Rehm BHA. Alginates: Biology and Applications. vol. 13. Berlin, Heidelberg: Springer Berlin Heidelberg; 2009. doi:10.1007/978-3-540-92679-5.

[57] Davidovich-Pinhas M, Bianco-Peled H. A quantitative analysis of alginate swelling. Carbohydr Polym 2010;79:1020–7. doi:10.1016/j.carbpol.2009.10.036.

[58] Bohren FC, Hoffman DR. Absorption and scattering of light by small particles. Wiley. New York: 1983.

[59] Maire E, Buffière JY, Salvo L, Blandin JJ, Ludwig W, Létang JM. On the Application of X-ray Microtomography in the Field of Materials Science. Adv Eng Mater 2001;3:539–46. doi:10.1002/1527-2648(200108)3:8<539::AID-ADEM539>3.0.CO;2-6.

[60] Salvo L, Cloetens P, Maire E, Zabler S, Blandin JJ, Buffi??re JY, et al. X-ray micro-tomography an attractive characterisation technique in materials science. Nucl Instruments

554 Methods Phys Res Sect B Beam Interact with Mater Atoms 2003;200:273–86.
555 doi:10.1016/S0168-583X(02)01689-0.
556 [61] Fainerman VB, Lucassen-Reynders EH, Miller R. Adsorption of surfactants and proteins
557 at fluid interfaces. Colloids Surfaces A Physicochem Eng Asp 1998;143:141–65.
558 doi:10.1016/S0927-7757(98)00585-8.
559 [62] Doublier JL, Garnier C, Renard D, Sanchez C. Protein-polysaccharide interactions. Curr
560 Opin Colloid Interface Sci 2000;5:202–14. doi:10.1016/S1359-0294(00)00054-6.
561 [63] Ye A, Hemar Y, Singh H. Influence of polysaccharides on the rate of coalescence in oil-
562 in-water emulsions formed with highly hydrolyzed whey proteins. J Agric Food Chem
563 2004;52:5491–8. doi:10.1021/jf030762o.
564 [64] Eugénie S de P, Fabrice D, Gérard C, Samir M. Effect of bulk viscosity and surface
565 tension kinetics on structure of foam generated at the pilot scale. Food Hydrocoll
566 2014;34:104–11. doi:10.1016/j.foodhyd.2012.12.001.
567 [65] Yang X, Foegeding EA. The stability and physical properties of egg white and whey
568 protein foams explained based on microstructure and interfacial properties. Food
569 Hydrocoll 2011;25:1687–701. doi:10.1016/j.foodhyd.2011.03.008.
570 [66] Ström A, Lundin L, Morris E, Williams MAK. Relation between Rheological Properties
571 of Pectin Gels and Pectin Fine Structure 2012;20:159–66.
572 [67] Pugh RJ. The stability/instability of bubbles and foams. Bubble Foam Chem. Cambridge,
573 Cambridge: Cambridge University Press; 2016, p. 220–68.
574 doi:10.1017/CBO9781316106938.008.
575 [68] Murray BS. Stabilization of bubbles and foams. Curr Opin Colloid Interface Sci
576 2007;12:232–41. doi:10.1016/j.cocis.2007.07.009.
577 [69] Ye A. Complexation between milk proteins and polysaccharides via electrostatic
578 interaction: Principles and applications - A review. Int J Food Sci Technol 2008;43:406–
579 15. doi:10.1111/j.1365-2621.2006.01454.x.
580 [70] Rodriguez Patino JM, Pilosof AMR. Protein-polysaccharide interactions at fluid
581 interfaces. Food Hydrocoll 2011;25:1925–37. doi:10.1016/j.foodhyd.2011.02.023.
582 [71] Gibson LJ, Ashby MF. Cellular Solids: Structure and Properties. Pergamon. New York:
583 1997.
584 [72] Kloxin AM, Kloxin CJ, Bowman CN, Anseth KS. Mechanical Properties of Cellularly
585 Responsive Hydrogels and Their Experimental Determination. Adv Mater 2010;22:3484–
586 94. doi:10.1002/adma.200904179.
587 [73] Gooch JW. Law of Mixtures. Encycl. Dict. Polym., New York, NY: Springer New York;
588 2011, p. 421–421. doi:10.1007/978-1-4419-6247-8_6810.
589 [74] Xanthos M. Polymers and Polymer Composites. Funct. Fill. Plast., Weinheim, FRG:
590 Wiley-VCH Verlag GmbH & Co. KGaA; 2005, p. 1–16. doi:10.1002/3527605096.ch1.
591 [75] Voigt W. Ueber die Beziehung zwischen den beiden Elasticitätsconstanten isotroper
592 Körper. Ann Phys 1889;274:573–87. doi:10.1002/andp.18892741206.
593 [76] Nielsen LE. Simple theory of stress-strain properties of filled polymers. J Appl Polym Sci
594 1966;10:97–103. doi:10.1002/app.1966.070100107.
595 [77] Hölzl K, Lin S, Tytgat L, Van Vlierberghe S, Gu L, Ovsianikov A. Bioink properties
596 before, during and after 3D bioprinting. Biofabrication 2016;8:32002. doi:10.1088/1758-
597 5090/8/3/032002.
598 [78] Murphy S V, Atala A. 3D bioprinting of tissues and organs. Nat Biotechnol 2014;32:773–
599 85. doi:10.1038/nbt.2958.

[79] Chang R, Nam J, Sun W. Direct cell writing of 3D microorgan for in vitro pharmacokinetic model. Tissue Eng Part C Methods 2008;14:157–66. doi:10.1089/ten.tec.2007.0392.

[80] Verboven P, Herremans E, Helfen L, Ho QT, Abera M, Baumbach T, et al. Synchrotron X-ray computed laminography of the three-dimensional anatomy of tomato leaves. Plant J 2015;81:169–82. doi:10.1111/tpj.12701.

[81] Wuyts N, Palauqui JC, Conejero G, Verdeil JL, Granier C, Massonnet C. High-contrast three-dimensional imaging of the Arabidopsis leaf enables the analysis of cell dimensions in the epidermis and mesophyll. Plant Methods 2010;6:17. doi:10.1186/1746-4811-6-17.

[82] Coate JE, Luciano AK, Seralathan V, Minchew KJ, Owens TG, Doyle JJ. Anatomical, biochemical, and photosynthetic responses to recent allopolyploidy in glycine dolichocarpa (fabaceae). Am J Bot 2012;99:55–67. doi:10.3732/ajb.1100465.

Table 1 Overview of the production steps.

Timeline	Production step	Description
Day 0	Preparation of maceration and buffer solutions	Isotonic solutions used for the cell isolation
Day 1	Isolation of Lamb's lettuce cells	Incubation of lettuce leaves into maceration buffer Determination of cell viability
	Preparation of pectin solution	Dilution of LM pectin into buffer solution
Day 2	Bio-ink preparation	Incubation of cell suspension into $CaCl_2$ buffer solution High stirring of pectin solution with or without BSA Mixing of cell/$CaCl_2$ suspension into pectin solution
	3D printing	Extrusion deposition of bio-ink layer by layer at room temperature Incubation in $CaCl_2$ crosslink solution
	Confocal microscopy	Visualization of alive and dead cell in the 3D printed objects and viability characterization
Day 3	Micro computed tomography	Visualization and characterization of the porosity in the 3D printed objects
	Photography	Determination of the build quality of the printed objects
	Compression test	Measurement of the mechanical properties of the printed objects

Table 2 Bio-ink compositions

Label	LM pectin g/L	$CaCl_2$ mM	BSA g/L	Lamb's lettuce cell suspension % (v/v)
15p_ref	15	6.5	0	0
15p_BSA_ref	15	6.5	2	0
15p_cell	15	6.5	0	50
15p_BSA_cell	15	6.5	2	50
35p_ref	35	10	0	0
35p_BSA_ref	35	10	2	0
35p_cell	35	10	0	50
35p_BSA_cell	35	10	2	50

Table 3 Porosity (ϕ) ± standard error of 3D printed objects.

Samples	ϕ %
15p_ref	1.38 ± 0.16
15p_BSA_ref	26.42 ± 0.45
15p_cell	0.30 ± 0.24
15p_BSA_cell	23.15 ± 0.79
35p_ref	0.46 ± 0.07
35p_BSA_ref	5.25 ± 0.09
35p_cell	0.02 ± 0.02
35p_BSA_cell	1.51 ± 0.21

Table 4 Viability ± standard error (%) of the cell suspensions after isolation (initial suspension) and after the decantation into the $CaCl_2$ solutions with and without 0.2% (w/v) BSA. For bio-ink made of 15 g/L pectin, the cells were decanted into 13 mM$CaCl_2$ solution. For bio-ink made of 35 g/L pectin, the cells were decanted into 20 mM $CaCl_2$ solution.

Batch	**Initial suspension**	**After 20 min in 13 or 20 mM $CaCl_2$ + 0.2 % (w/v) BSA + buffer**	**After 20 min in 13 or 20 mM $CaCl_2$ + buffer**
For bio-inks made of 15 g/L pectin	85.7 ± 5.4	82.2 ± 5.0	81.4 ± 5.6
For bio-inks made of 35 g/L pectin	84.3 ± 4.7	77.7 ± 5.1	81.2 ± 7.2

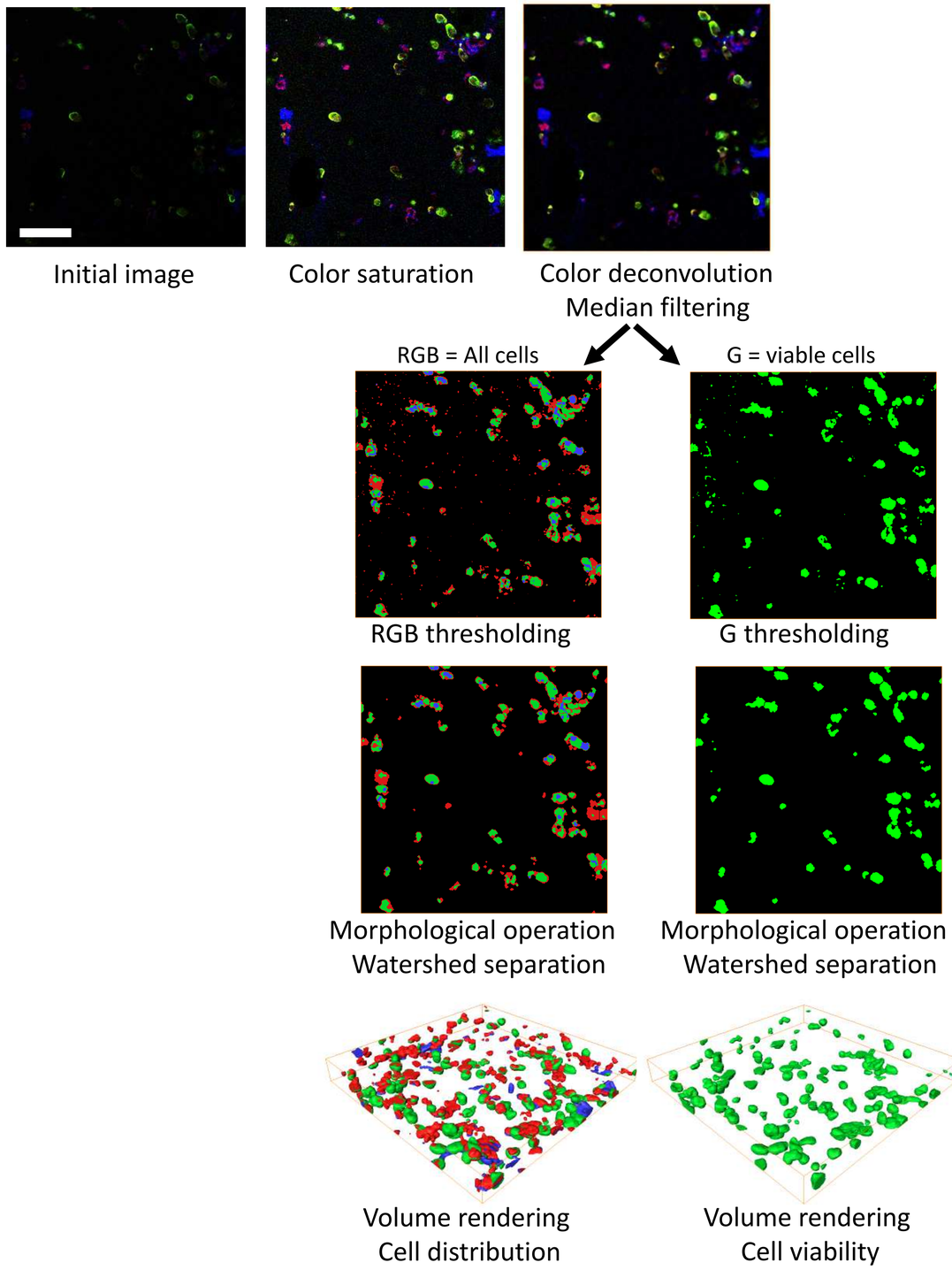
Initial image
Color saturation
Color deconvolution
Median filtering
RGB = All cells
G = viable cells
RGB thresholding
G thresholding
Morphological operation
Watershed separation
Morphological operation
Watershed separation
Volume rendering
Cell distribution
Volume rendering
Cell viability

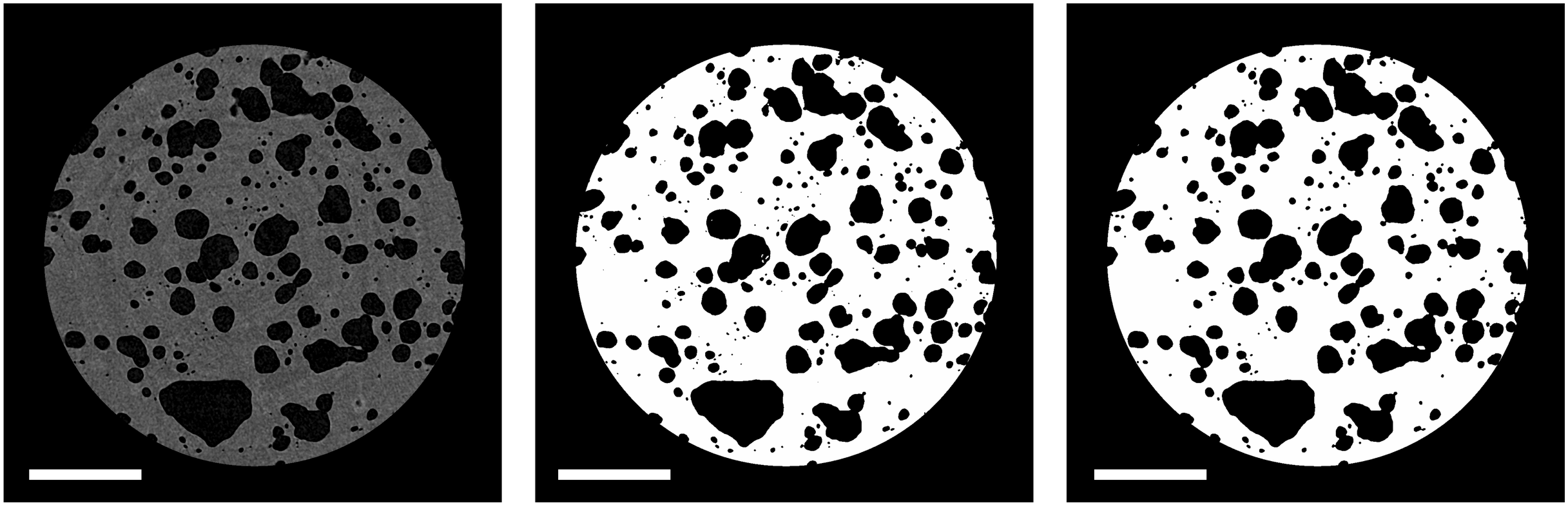

(a) (b) (c)

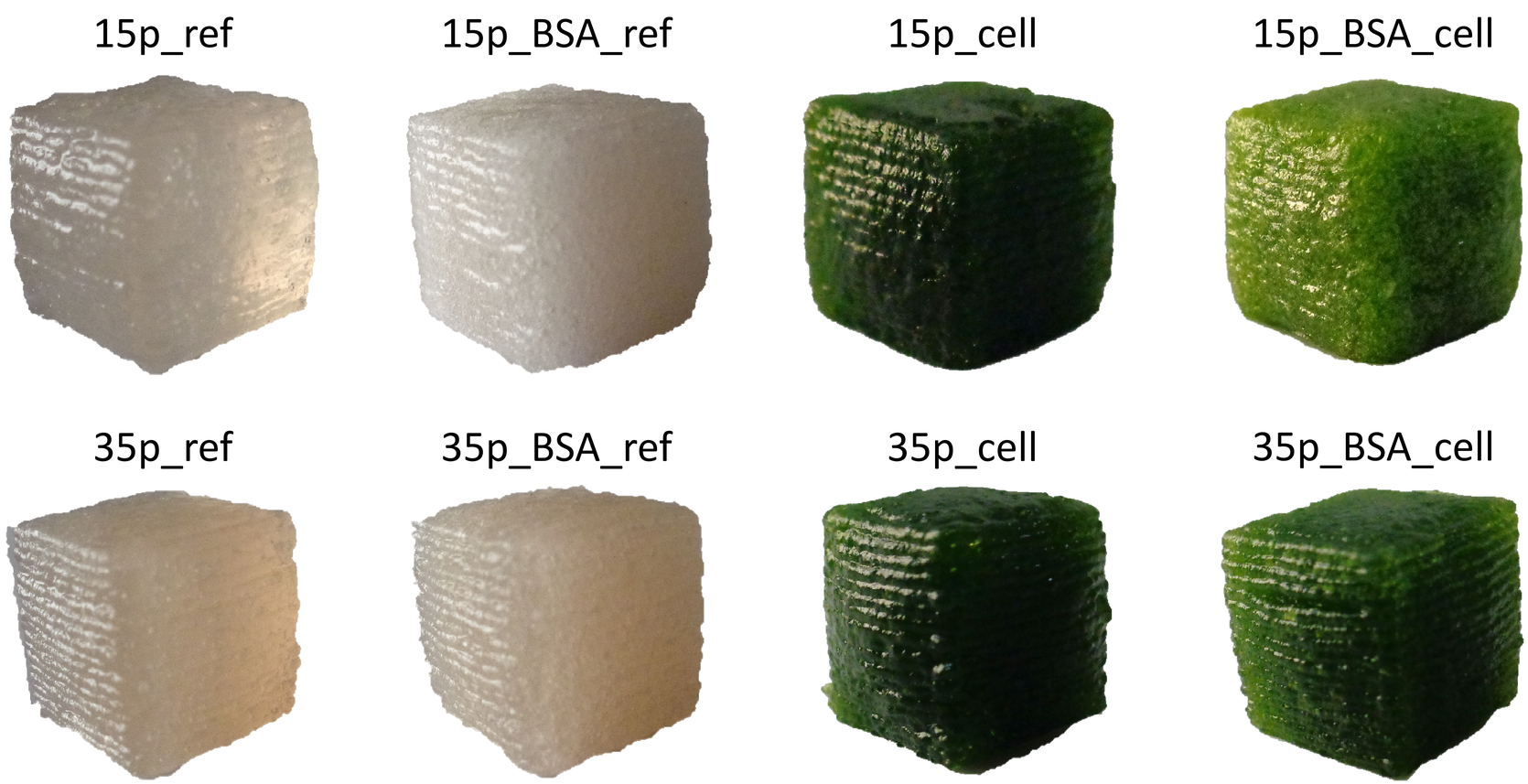
15p_ref
15p_BSA_ref
15p_cell
15p_BSA_cell
35p_ref
35p_BSA_ref
35p_cell
35p_BSA_cell

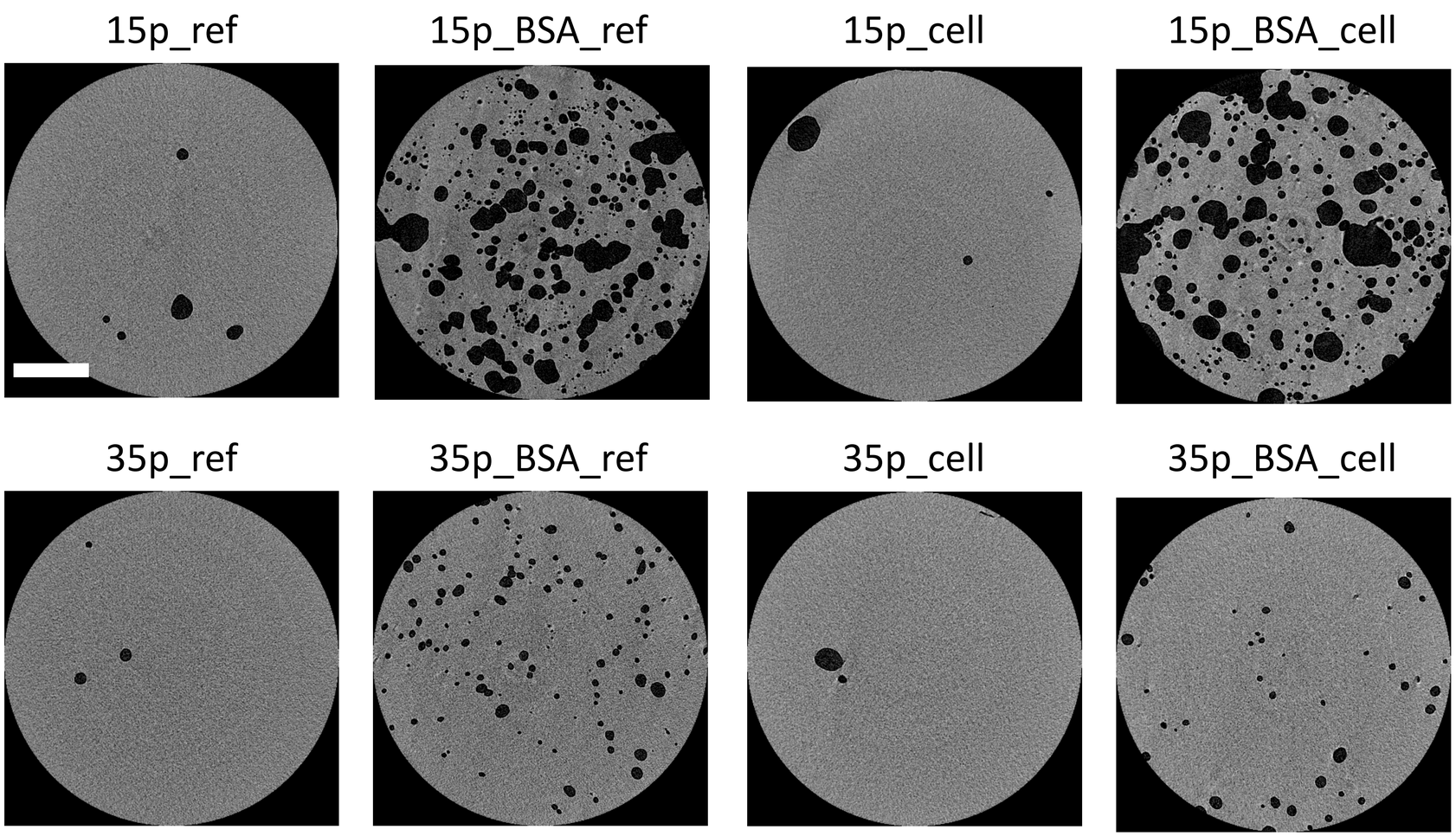
15p_ref
15p_BSA_ref
15p_cell
15p_BSA_cell
35p_ref
35p_BSA_ref
35p_cell
35p_BSA_cell

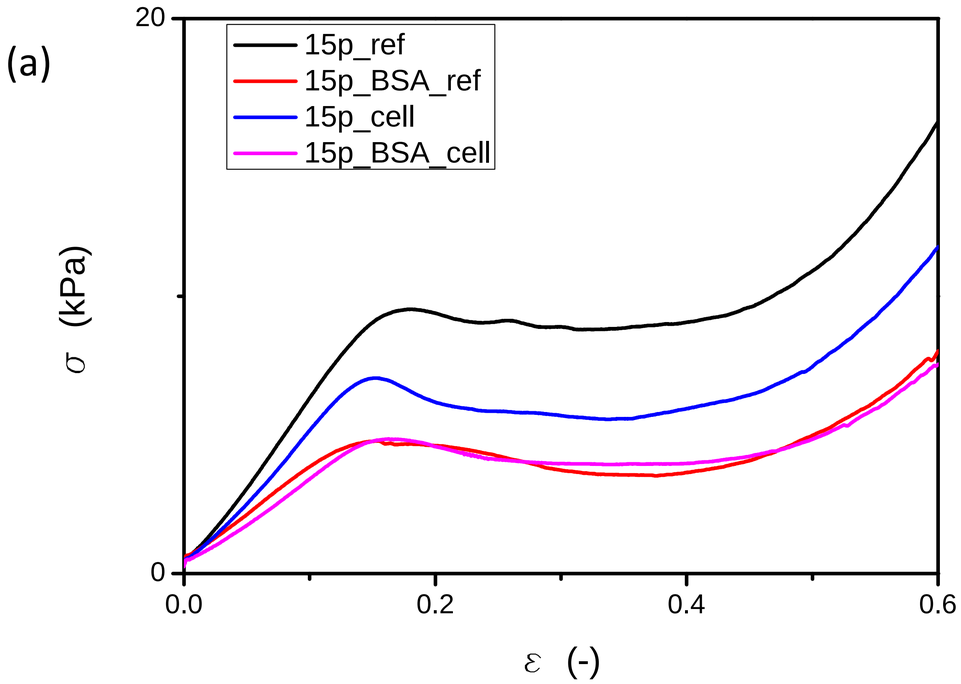
(a)
15p_ref
15p_BSA_ref
15p_cell
15p_BSA_cell
σ (kPa)
ε (-)
0
20
0.0
0.2
0.4
0.6

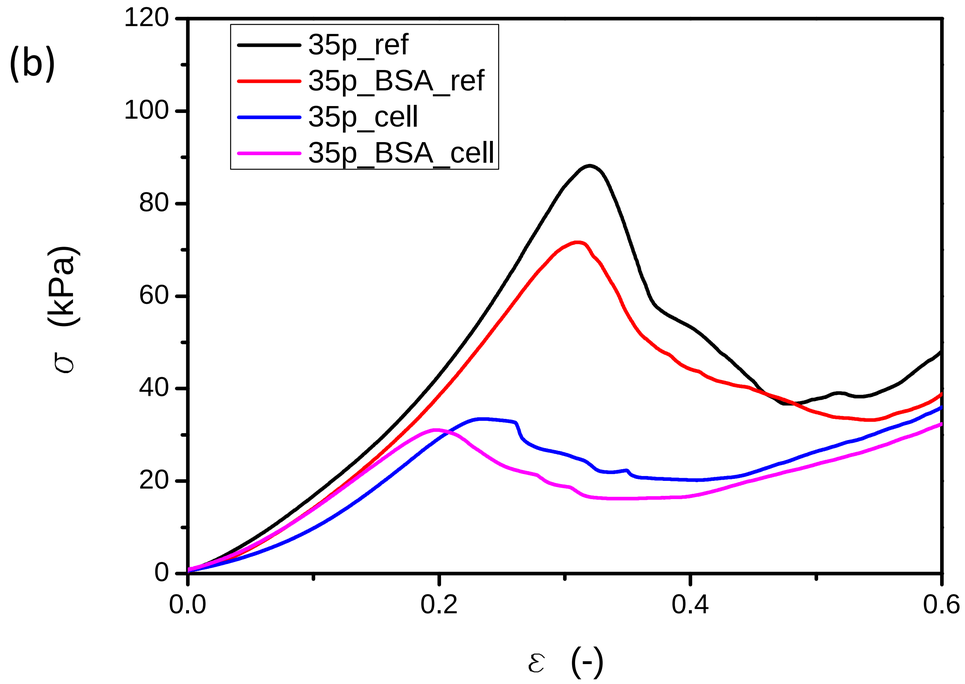
(b)
35p_ref
35p_BSA_ref
35p_cell
35p_BSA_cell
σ (kPa)
ε (-)
0
20
40
60
80
100
120
0.0
0.2
0.4
0.6

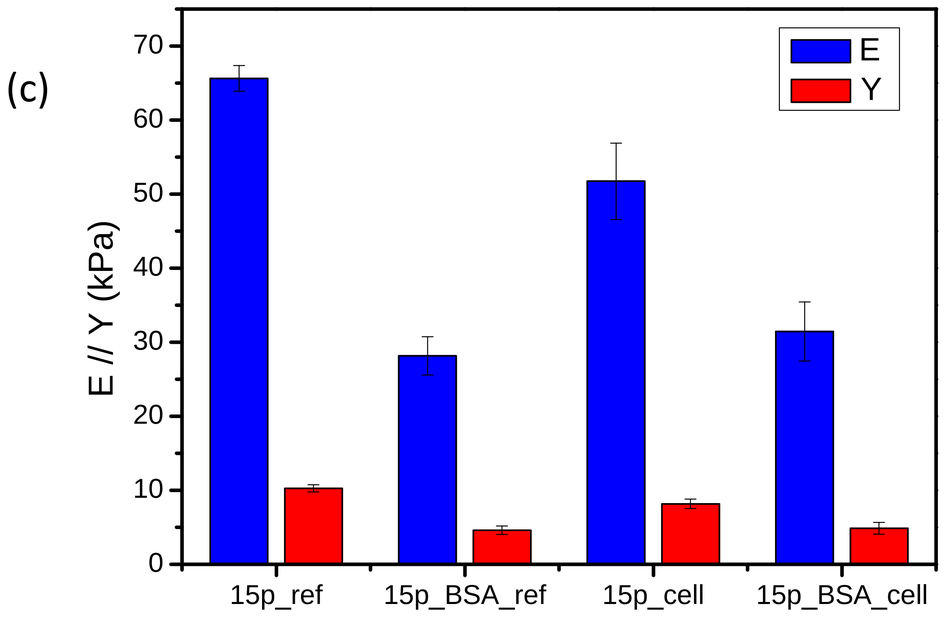
(c)
E
Y
E // Y (kPa)
0
10
20
30
40
50
60
70
15p_ref
15p_BSA_ref
15p_cell
15p_BSA_cell

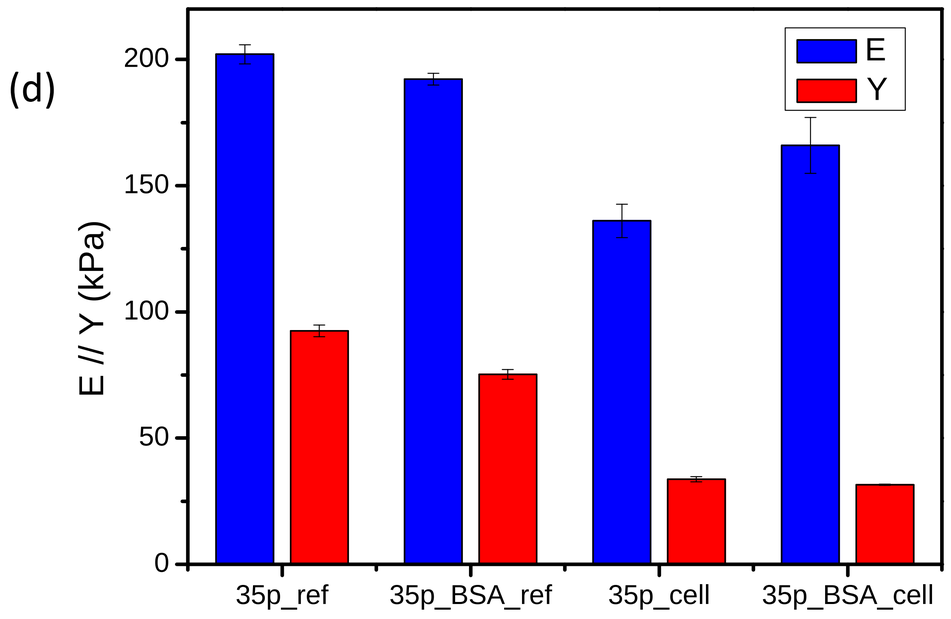
(d)
E
Y
E // Y (kPa)
0
50
100
150
200
35p_ref
35p_BSA_ref
35p_cell
35p_BSA_cell

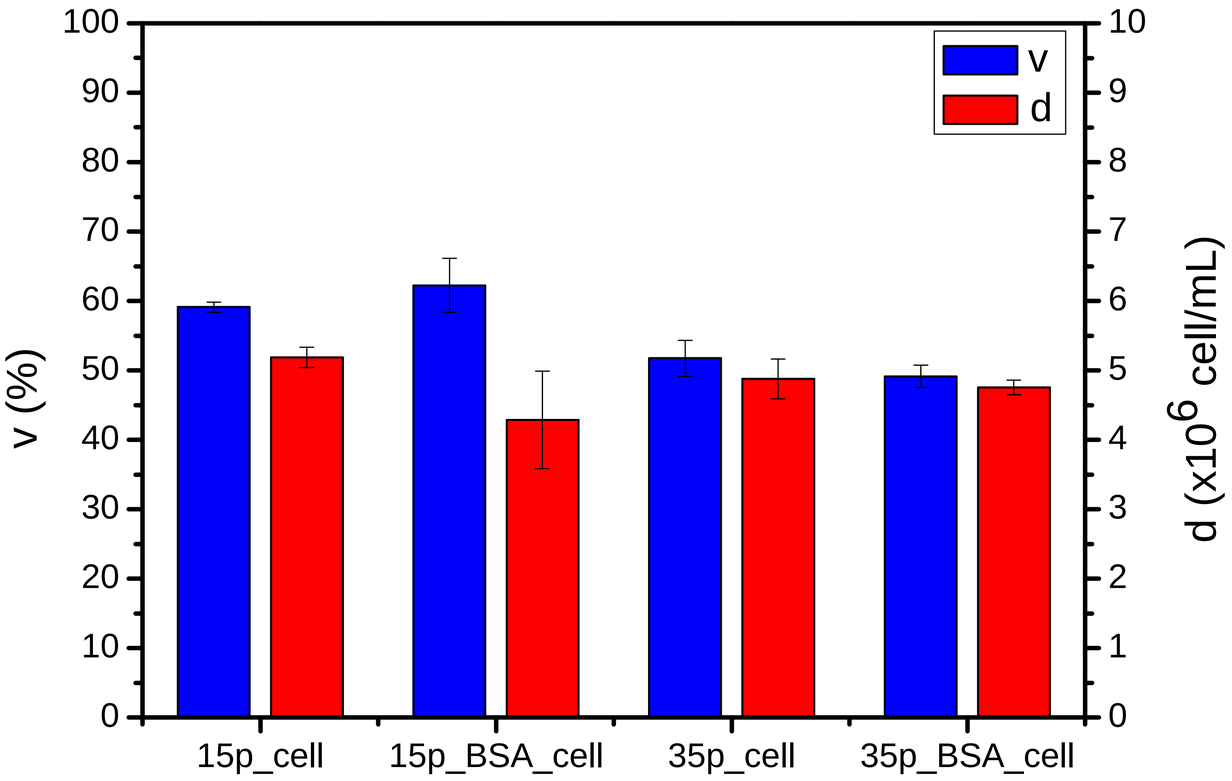
v
d
v (%)
d (x10^6 cell/mL)
100
90
80
70
60
50
40
30
20
10
0
10
9
8
7
6
5
4
3
2
1
0
15p_cell
15p_BSA_cell
35p_cell
35p_BSA_cell

15p_cell

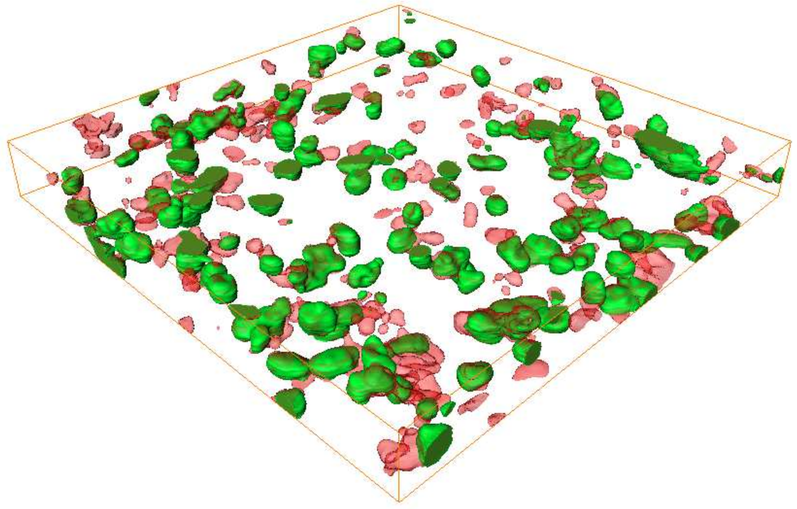

15p_BSA_cell

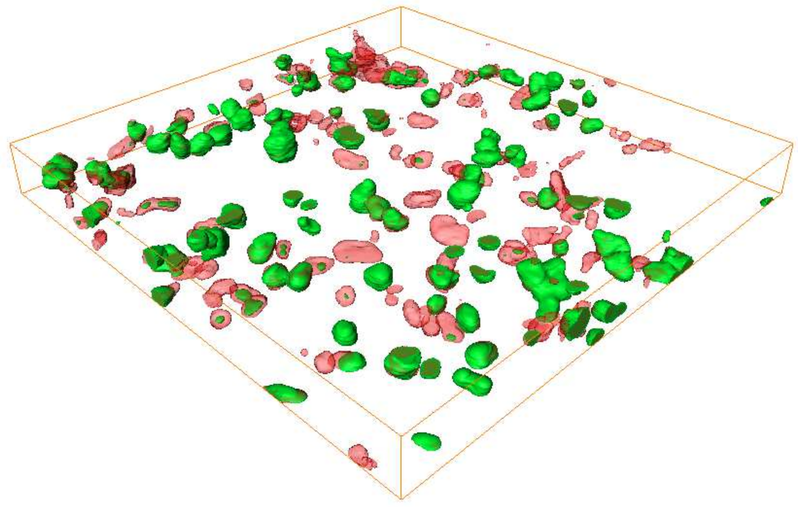

35p_cell

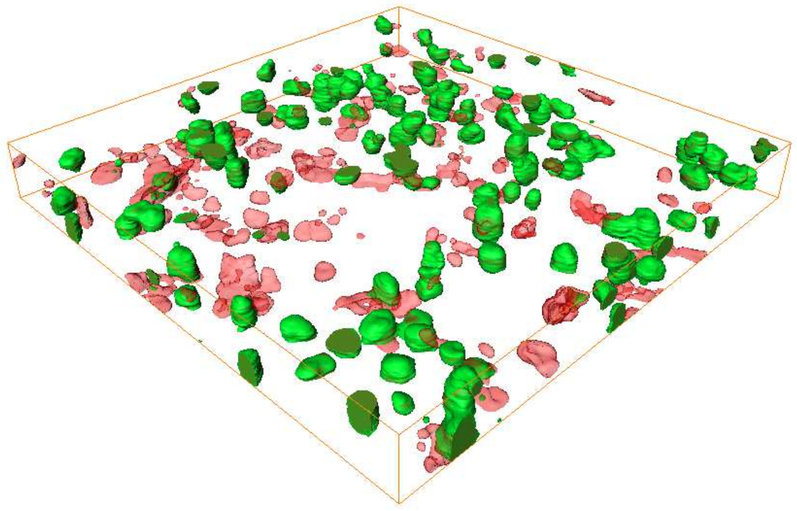

35p_BSA_cell

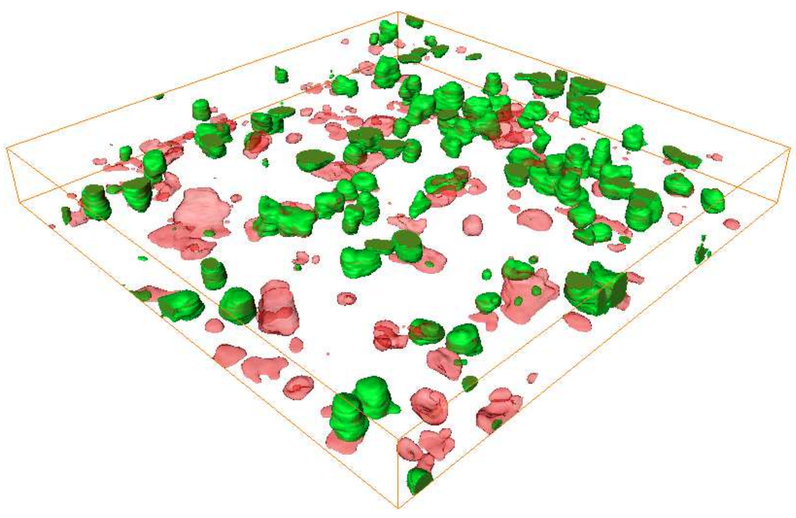

Highlights

- Objects were 3D printed using pectin gel and encapsulated alive plant cells.
- Objects with variable properties were printed by changing the bio-ink composition.
- Bovine Serum albumin increased the air fraction in the printed gel matrix.
- The increase of pectin concentration increased mechanical properties of printed object.
- The viability of encapsulated plant cells depended on the pectin concentration.